Mathematical Biosciences and Engineering

MBE, 20 (11): 20002–20024.
DOI: 10.3934/mbe.2023886
Received: 08 August 2023
Revised: 23 October 2023
Accepted: 30 October 2023
Published: 02 November2023

http://www.aimspress.com/journal/MBE

Research article

A gait stability evaluation method based on wearable acceleration sensors

Xuecheng Weng[1], Chang Mei[1], Farong Gao[1,*], Xudong Wu[2], Qizhong Zhang[1] and Guangyu Liu[1]

[1] School of Artificial Intelligence, Hangzhou Dianzi University, Hangzhou 310018, China

[2] Department of Orthopaedics, Zhoushan Hospital of Traditional Chinese Medicine, Zhoushan 316000, China

* **Correspondence:** Email: frgao@hdu.edu.cn; Tel: +8657186919108.

Abstract: In this study, an accurate tool is provided for the evaluation of the effect of joint motion effect on gait stability. This quantitative gait evaluation method relies exclusively on the analysis of data acquired using acceleration sensors. First, the acceleration signal of lower limb motion is collected dynamically in real-time through the acceleration sensor. Second, an algorithm based on improved dynamic time warping (DTW) is proposed and used to calculate the gait stability index of the lower limbs. Finally, the effects of different joint braces on gait stability are analyzed. The experimental results show that the joint brace at the ankle and the knee reduces the range of motions of both ankle and knee joints, and a certain impact is exerted on the gait stability. In comparison to the ankle joint brace, the knee joint brace inflicts increased disturbance on the gait stability. Compared to the joint motion of the braced side, which showed a large deviation, the joint motion of the unbraced side was more similar to that of the normal walking process. In this paper, the quantitative evaluation algorithm based on DTW makes the results more intuitive and has potential application value in the evaluation of lower limb dysfunction, clinical training and rehabilitation.

Keywords: gait assessment; acceleration sensor; joint activity; stability; dynamic time warping

1. Introduction

The walking ability of humans integrates functions of the nervous, musculoskeletal and

physiological brace systems as well as their coupling [1]. Thus, human upright walking is a continuous and variable complex process requires constant stability. Gait is a comprehensive characteristic of human walking behavior, influenced in varying degrees by changes of human physiological function, pathology and even mental state [2]. Due to this importance, gait analysis has been widely applied. For example, gait can represent the characteristics of human identity information. Combining gait analysis with other forms of identity recognition will make significant contributions in areas such as privacy protection and public safety [3,4]. In addition, the reflection of gait on human health and pathological characteristics makes studying participants' basic lower limb function crucial for developing and improving clinical evaluation systems [5]. Among a range of features that describe gait, the stability of leg walking has been shown to be an important measure which allows distinguishing healthy and pathological features [6–8]. Therefore, in recent years, the use of gait stability for disease evaluation and postoperative recovery is being reported in increasing frequency [9,10].

Gait signals are usually derived through kinematic and bioelectrical signal recording, videos and images. In addition, there have been several advanced sensors that can improve the fidelity in data collection, but have not yet been applied and validated in gait analysis [11–15]. Analysis systems proposed in the past are not suitable for routine clinical use due to their harsh application conditions and cumbersome process [16–18]. Observation scales are also widely used in gait assessment, but their use often depends on the subjective judgment of clinicians and cannot be used to quantify the walking status of lower limbs [19,20]. In order to solve the above problems, wearable sensors have been widely used in various studies in recent years to evaluate gait during lower limb movement [21,22]. Among these sensors, the acceleration sensor is widely used in the evaluation of lower limb motion because of its advantages in the continuous modal acquisition of human motion information [23–25]. Studies have shown that wearable sensors are quite suitable for evaluating temporal and spatial parameters of human gait during activities of daily living. In recent years, gait evaluation methods based on wearable sensors have been proved to be reliable [26–28].

Salatino et al. [29] used wearable acceleration sensors to study the influence of Down's syndrome on lower limb joint movement during walking. The study revealed that patients with Down syndrome have limited range of motion in the lower extremity joints, leading to walking instability. Johansson et al. [30] used triaxial accelerometers to assess the fall risk of elderly participants during walking, and their study showed that elderly women walk more erratically and have a higher risk of falling than men. Nelm et al. [31] used a triaxial accelerometer to evaluate lower extremity kinematic stability before and after hip arthroplasty. Their approach helps identify significant improvements in lower extremity movement stability after hip replacement surgery. Tamburini et al. [32] studied the influence of different environments on gait stability based on inertial sensors. The results of the study showed that for healthy adults, the experimental environment and test conditions had an effect on the gait variability index but no significant effect on the stability index. Additionally, in some studies, inertial sensors assessed gait performance in Parkinson's patients [33–35]. With the above study, it was found that that gait parameters included the coefficient of variation [36], step length, step width, time interval between two steps, joint angles as well as the nonlinear features [37], and we have studied gait events with the linear and nonlinear features in our previous work [16]. In current gait analysis, linear features are as the main indicators for evaluating stability levels due to their convenience and intuitiveness, but these are often not sufficient to account for the stability of the human body in a continuous walking state, which may lead to the neglect of some data during the

analysis process. These methods cannot provide behavioral information about other joints or quantitative information for complex lower extremity movements, because they cannot capture spatiotemporal complex gait cycles [38]. Considering the linear and nonlinear relationships of parameters, many deep learning methods of data processing have achieved success in different fields for situations involving a large number of different data types, as well as the parameter distribution differences [39–43]. In the current gait analysis field, a large number of machine learning methods have been developed to deal with different gait research problems. For gait feature extraction and classification, artificial neural network (ANN), deep neural network (DNN), extreme learning machine (ELM), transformer and other methods have been proved to be effective [44–46]. However, there are few quantitative evaluation methods for gait. Other common quantitative gait evaluation methods include the autocorrelation function method [47] and the similarity evaluation method based on the nearest neighbor analysis in terms of the Euclidean distance [48]. These methods can only be used for stability evaluation through distance calculation on sequences of equal length. However, when the human body is walking, not only the duration of each step may differ from that of other steps, but also duration of adjacent gait cycles shows variation. Therefore, it is difficult to calculate the difference between two gait motion samples using Euclidean distance-based methods.

Considering the above problems, in this paper a new quantitative analysis method is proposed for the assessment of lower extremity motor stability. Through the use of dynamic programming for sequence alignment and thus minimization of the effects of time axis lag and distortion caused by velocity changes, dynamic time warping (DTW) can be used to analyze any data that are transformed into a linear representation. The DTW algorithm was first mainly used for template matching of video, audio and image data, and now its application in the field of sound recognition is very mature [49]. Due to the characteristics and advantages of DTW, many researchers have recently begun to apply the DTW algorithm to human movement assessment and rehabilitation physiotherapy guidance. Semblantes et al. [50] used the DTW algorithm and dichotomy to distinguish whether an action is correct. Su et al. [51] used the DTW algorithm to classify a patient's performance into three levels: poor, good and excellent, through the calculation of the minimum cumulative distance between the measured object and the measurement template. The above methods focus on evaluating actions subjectively or qualitatively and the results obtained using the DTW algorithm are not converted into quantitative scores. Minsu Jang et al. [52] used the DTW algorithm combined with the LMA (laban movement analysis) evaluation method to convert the Laban movement analysis. Osgouei et al. [53] proposed an evaluation method based on DTW algorithm using Kinect camera to quantitatively evaluate the effect of rehabilitation exercise.

The evaluation of gait state is of great significance in clinical diagnosis and rehabilitation, and a method that is more conducive to promotion and application is urgently needed. Therefore, gait analysis through wearable acceleration sensors with lower cost and more convenient application, is an important field in current gait research. In addition, to improve the feasibility of wearable accelerometers in potential clinical gait evaluation, we propose a quantitative gait stability evaluation method. The contributions are summarized as follows.

1). The DTW algorithm is proposed to be used for the evaluation of the gait stability based on wearable acceleration sensors.

2). The normal and abnormal gait signals of healthy subjects are compared and gait metrics are obtained.

3). The theoretical and experimental results show that this study provides a quantifiable method

for gait stability evaluation, which can obtain more intuitive quantitative scores.

The remaining chapters are organized as follows. Section 2 describes the proposed method, Section 3 is the experimental results and discussion, and the conclusion is drawn in Section 4.

2. Methods

For the experiments of this paper, acceleration sensors were used to collect acceleration signals from participants during the various parts of the experiment. A joint brace was used to limit the movement of the joint to simulate the symptoms of decreased joint range of motion. In order to reduce the signal noise and the collected data's quality for subsequent processing, a smoothing function is first introduced to for wavelet-based de-noising. Then, the normal walking data are used to establish the stride template, and the walking data after the stride template has been established and the joints have been braced are matched using the DTW algorithm depending on the experimental requirements. After that, the data processed using the DTW algorithm are introduced sequentially into the stability measurement equation to obtain the measurement index. Finally, the experimental data and stability measurement results are discussed and analyzed. Figure 1 shows the research process and method.

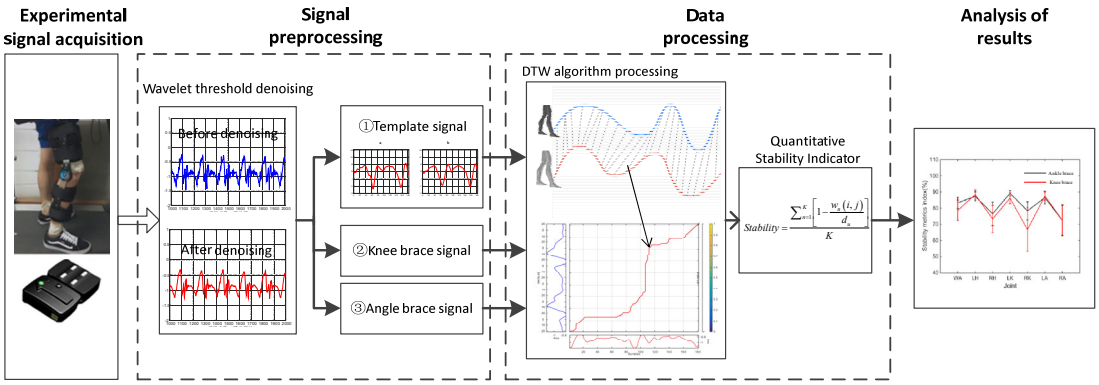

Figure 1. Research process and method.

2.1. Experiments

2.1.1. Experiment preparation

In this study, a walking experiment was used in gait evaluation. During the experiment, the triaxial acceleration sensor was fixed on the back waist, left and right hip joints, left and right knee joints and left and right ankle joints of the eight participants. The acceleration sensors transmitted data to the computer through Bluetooth for processing. The triaxial acceleration sensors we selected from Delsys company with a sampling frequency set to 150 Hz. In addition, a treadmill as well as knee and ankle braces were used for this experiment. Figure 2 shows the joint brace and triaxial accelerometer.

We used a comparative experimental method between the normal group and the abnormal group to conduct a 2-minute walking test (2MW). The average preferred walking speed (PWS) [54] was set

as the walking speed on the treadmill. The experiment was conducted under the following conditions: Normal walking, walking with knee brace on unilateral side and walking with an ankle brace on the unilateral side. All the experiments were repeated three times for each of the eight participants.

Figure 2. Joint brace and three-axis accelerometer. (a: Knee Brace; b: Ankle Brace; c: Three-axis accelerometer).

2.1.2. Experiment steps

In this study, a comparison experiment between normal walking and walking with a joint brace was performed. The subject fixed the triaxial acceleration sensors at the corresponding joints. First, multiple groups of normal walking signals were acquired to establish the stride templates. After that, the participants were braced at the joints to simulate the gait instability caused by the influence of joints, and the walking experiment was repeated. The accelerometer transmitted data to the computer via Bluetooth for data processing.

2.2. Preprocessing of acceleration signal

When acquiring the gait acceleration data, the accelerometer and the acquisition box communicate through Bluetooth connection. The process is easily affected by external power frequency noise, high frequency interference, human tremor and other inherent and environmental factors. This noise disturbance is tangled with the acceleration signal of gait motion, causing partial distortions to the collected signal. Therefore, in order to reduce environmental and human factors interference, the wavelet threshold de-noising algorithm [55] was utilized to filter the noise from the data.

2.2.1. Deviation correction of acceleration signal

The measurement errors of three-axis accelerometer mainly include heating and noise errors, accelerometer installation errors and non orthogonal errors between axes. In order to reduce these errors, various errors are compensated and corrected to improve accuracy. In the actual experiment, due to the wearing position and other factors, there is a certain angle between the vertical axis direction of the accelerometer and the gravity acceleration direction.

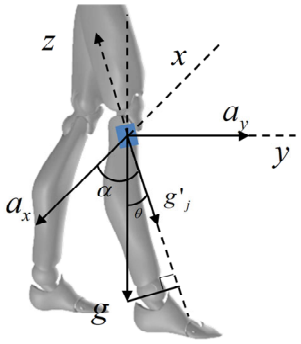

Figure 3. The relationship between the gravity acceleration direction and the position of the three-axis accelerometer.

The three axes of the three-axis accelerometer are respectively represented by x, y, z, and their corresponding acceleration values are a_x, a_y and a_z. Assume that the included angle between the gravity direction and the xy plane of the acceleration sensor is θ (pitch angle), and the projection of the gravity acceleration direction on the xy plane forms an angle α (roll angle) with the x-axis of the sensor, where g'_j is the projection of the gravity acceleration on the xy plane. As shown in Figure 3, the relationship between the gravity acceleration direction and the position of the three-axis accelerometer.

When measuring the acceleration values in three directions of the three-axis acceleration sensor at rest are a_{jx}, a_{jy}, a_{jz} and the gravitational acceleration g is known.

$$g'_j = \sqrt{\alpha_{jx}^2 + \alpha_{jy}^2} \tag{1}$$

$$\cos\theta = \frac{g'_j}{g} \tag{2}$$

$$\cos\alpha = \frac{a_{jx}}{g'_j} \tag{3}$$

The included angles θ and α can be calculated by the Eqs (2) and (3). It can be obtained that the actual acceleration values A_x, A_y, A_z are,

$$A_x = a_y \sin\theta\cos\alpha - a_z \sin\theta\cos\alpha + a_z \cos\theta\sin\alpha \tag{4}$$

$$A_y = a_y \sin\theta\cos\alpha + a_z \sin\theta\sin\alpha - a_z \cos\theta\cos\alpha \tag{5}$$

$$A_z = a_x \sin\theta - a_y \cos\theta + a_z \cos\theta \tag{6}$$

where A_x is the acceleration in the direction of the coronal axis, A_y is the acceleration in the direction of the sagittal axis, and A_z is the acceleration in the direction of gravity.

2.2.2. Wavelet threshold de-noising

Wavelet threshold functions mainly include soft threshold functions, hard threshold functions and soft-hard compromise functions. Soft threshold functions are generally continuous, but there is a constant deviation which directly affects the reconstructed signal's approximation degree of the original one. Hard threshold methods are better than soft ones in the mean variance sense. However, the filtered signal will produce additional oscillations and jump points, thus disturbing the smoothness of the original signal. Although the soft and hard threshold compromise functions offer some improvements over the respective methods, they only reduce the bias in the soft threshold but do not eliminate it completely. To overcome the shortcomings of the above threshold functions, a smoothness function is introduced to improve them as follows,

$$f_T(\omega_{jk})=\begin{cases}\omega_{jk} & |\omega_{jk}|\geq T_{jk}+\varepsilon T_{jk}\\ 0 & |\omega_{jk}|<T_{jk}-\varepsilon T_{jk}\\ \operatorname{sgn}(\omega_{jk})\dfrac{(|\omega_{jk}|-T_{jk}+\varepsilon T_{jk})^2((\varepsilon+1)^2T_{jk}^2-T_{jk}|\omega_{jk}|)}{4\varepsilon^3T_{jk}^3} & T_{jk}-\varepsilon T_{jk}<|\omega_{jk}|<T_{jk}+\varepsilon T_{jk}\end{cases}, \tag{7}$$

where $f_T(\omega_{jk})$ is the wavelet coefficient after threshold processing; T_{jk} is the k-th high frequency wavelet coefficient component threshold in the j-th layer; ω_{jk} is the k-th high frequency coefficient in the j-th layer; and ε is a constant with $\varepsilon\subset(0,1)$. The addition of the cubic equation of one variable tangent to two straight lines, namely to $|T_{jk}+\varepsilon T_{jk}|$ and $|T_{jk}-\varepsilon T_{jk}|$, compensates for the non-smooth hard threshold function and eliminates the problem of constant deviation at $|\omega_{jk}|\geq T_{jk}+\varepsilon T_{jk}$. However, it also increases the computational complexity.

2.3. Division of step and establishment of average step

Converting human gait into specific data for analysis based in basic characteristics, such as step and stride, can be achieved through data analysis. Therefore, it is significant to measure the gait characteristic parameters of human walking quantitatively so as to analyze human gait motion. During walking, the linear length of the same foot from the beginning of contact with the ground to the next contact with the ground is called stride. Gait characteristic parameters, such as stride and step length, can be calculated using the autocorrelation of acceleration [56].

A piecewise linear interpolation algorithm [57] was used to calculate the average stride length, at each joint, during normal walking for all participants. The method of piecewise interpolation as follows: First, the interpolation interval is divided into several small segments, and low-order interpolation is applied on each segment. Next, the interpolation polynomials at each small segment are stitched together as an interpolation function on the entire interval.

The length of the interpolation interval is $[1,N]$, where N is the sampling length of stride S. The interpolation interval is divided into q segments, $S=[s_0,s_1,s_2,\ldots s_q]$ where each segment is denoted by $[s_{i-1},s_i](i=1,2,...,q)$, a_i is the value of acceleration corresponding to s_i. The piecewise linear interpolation equation is,

$$S(s) = a_i + \frac{a_i - a_{i-1}}{a_i - a_{i-1}}(s - s_i) \tag{8}$$

The interpolation node is selected according to the following rule,

$$i = \begin{cases} 1 & s < s_0 \\ k & s_{k-1} < s \le s_k, \ (1 \le k \le q) \\ n & s > s_l \end{cases} \tag{9}$$

When the interpolation node set is $s_0, s_1, s_2, ..., s_{k-1}, s_k, ..., s_q$, each node from left to right is taken out in turn. If the interpolation point s does not exceed node s_1 (i.e., it lies between $[s_0, s_1]$), then nodes s_0, s_1 are considered to be linearly interpolated; otherwise, a sequential check is performed whether s exceeds s_2,.... Once it is found that s does not exceed a certain node s_i, this and the previous node s_{i-1}, are considered for linear interpolation. If s exceeded s_{q-1}, the interpolation nodes are set to s_q and s_{q-1} regardless if s exceeds s_q or not.

2.4. Dynamic time warping algorithm

The dynamic time warping algorithm is a method used to measure the similarity of the time series, which can minimize the effects of hysteresis and distortion caused by different speed. Compared with the deep neural network model, DTW does not need a large amount of early data for training, and consumes less resources in computing, which is more in line with the requirements of real-time [53,58]. In addition, the algorithm principle of DTW makes it more applicable when there is a reference template, which is consistent with the experiment used in this study.

During human walking, the acceleration signal is a periodic signal with the time elapsing. Within a gait cycle, its feature points are a two-dimensional sequence composed of time series and amplitude series. Therefore, in order to better measure the similarity between samples, we improved the DTW algorithm using two-dimensional sequence distance, and optimized the quantitative evaluation algorithm for similarity calculation.

If the time of the sample is denoted as X_t, Y_t and the amplitude is X_a, Y_a, the sample sequence is,

$$X = ((x_t(1), x_a(1)), ..., (x_t(m), x_a(m)) \tag{10}$$

$$Y = ((y_t(1), y_a(1)), ..., (y_t(n), y_a(n)) \tag{11}$$

The lengths of the two stride sequences X and Y are m and n, respectively. The single-point distance between x_i and y_i of the sequences X and Y is used to formulate a distance matrix W with a size of $m \times n$. The specific expression is,

$$W = \begin{bmatrix} w_{1,1} & w_{1,2} & \cdots & w_{1,n} \\ w_{2,1} & w_{2,2} & \cdots & w_{2,n} \\ \cdots & & w_{i,j} & \cdots \\ w_{m,1} & w_{m,2} & \cdots & w_{m,\mathrm{n}} \end{bmatrix}_{m \times n} \tag{12}$$

Point $w(i,j)$ in the distance matrix W corresponds to the Euclidean distance between each point x_i and y_i. The corresponding points act as similarity metrics between each point of sequence X and each point of sequence Y, with smaller distances corresponding the higher similarity degrees. The Euclidean distance equation between the two-dimensional sequences X and Y is,

$$w(i,j)=\sqrt{(x_t(i)-y_t(j))^2+(x_a(i)-y_a(j))^2} \tag{13}$$

Next, the global cost function D is derived, where element $d(i,j)$ represents the cumulative distance and is expressed as follows.

For the first row, $j\in[1,m]$

$$d(1,j)=\sum_{j=1}^{m} w(x_1,y_j) \tag{14}$$

For the first column, $i\in[1,n]$

$$d(i,1)=\sum_{i=1}^{n} w(x_i,y_1) \tag{15}$$

For the remaining elements, the cumulative distance $d(i,j)$ of $i\in[2,n]$, $j\in[2,m]$ can be expressed as follows. The cumulative distance $d(i,j)$ is the current grid point distance $w(i,j)$, that is, the sum of the Euclidean distance between points x_i and y_j, and the cumulative distance of the smallest element to that point,

$$d_{Distance}=w(i,j)+\min\{d_{i-1,j},d_{i,j-1},d_{i-1,j-1}\} \tag{16}$$

The dynamic regularization path P is the mapping relationship between the representative sequences X and Y,

$$P=<w_1,w_2,w_3,...,w_k> \tag{17}$$

The best path is the path that minimizes the cumulative distance. The path can be obtained through dynamic programming. The k th element along this path is denoted as w_k, where $k=1,...,K$ and $\max(m,n)<K<m+n-1$.

The DTW algorithm imposes certain restrictions on the routing path P, that is, the path be established, as long as the following three conditions are met.

(1) Boundary conditions

$$\begin{cases} w_1=(1,1) \\ w_k=(m,n) \end{cases} \tag{18}$$

Any two sequences may change, but the regular path P must start from the lower left corner w_1 of the grid and end at the upper right corner w_k.

(2) Continuity condition

For two points $w_{k-1}=(a',b')$ and $w_k=(a,b)$ in the regular path, the following must hold:

$$\begin{cases}(a-a') \le 1 \\ (b-b') \le 1\end{cases} \tag{19}$$

In the calculation process of the path, the points on the path cannot jump and can be matched only along adjacent points.

(3) Monotonic constraint

For two points $w_{k-1}=(a',b')$ and $w_k=(a,b)$ in the regular path, the following must hold:

$$\begin{cases}(a-a') \ge 0 \\ (b-b') \ge 0\end{cases} \tag{20}$$

The points on the cumulative distance matrix $d(i,j)$ must proceed monotonically with time.

2.5. Stability measure

The cumulative distance $d_{Distance}$ of shortest path in the DTW algorithm is considered a stability criterion, as lower values of this parameter value correspond to better gait stability. However, this parameter is not intuitive and illustrative. In this study, a normalized distance is defined within the range of 0% to 100% for the shortest path cumulative distance, where values closer to 100% indicate stronger walking stability, and the lower values represent worse stability. The key is to determine the threshold of the stability level d_u. The stability index equation is as follows,

$$Stability = \frac{\sum_{n=1}^{K}\left[1-\frac{w_n(i,j)}{d_u}\right]}{K} = 1-\frac{d_{Distance}}{K\cdot d_u} \tag{21}$$

$$d_u = \sqrt{L\cdot(x_u-y_l)^2} = \sqrt{L}\cdot w_u \tag{22}$$

where K is the path length of the minimum distance accumulated through the DTW, $w(i,j)$ is the Euclidean distance corresponding to the path in the distance matrix W and $d_{Distance}$ is the minimum cumulative distance. Determining the stability level threshold d_u is the key to determine whether the stability measure index can measure action stability accurately. If the threshold value is too small, the error will be amplified, while values too large will result in a lack of differentiation between stability levels. d_u can be obtained from Eq (22), where L is the number of dimensions contained in a sequence of samples, and w_u is the Euclidean distance between the upper and lower Euclidean distance. Then, Eq (22) is substituted into Eq (21) to obtain the stability measure,

$$Stability = 1-\frac{d_{Distance}}{K\cdot\sqrt{L}\cdot w_u} \tag{23}$$

3. Results and discussion

3.1. Experimental signal acquisition

To understand the effect of the decreased joint range of motion on gait stability, a walking

experiment was selected as the evaluation method used to limit the main joints (the knee and ankle joints are often used as the major joints for gait analysis [59]) to simulate the symptoms of decreased joint mobility due to pathological reasons. Eight healthy adults (age 23 ± 3 years) were selected for the experiment. All participants had no neurological or orthopedic disease, neither had they suffered a fall in year preceding the experiment or had knee or ankle surgery in the past three years, so as to minimize the impact of external factors on the experiment.

We conduct the two-minute walking test (2MW), it is widely used in medical gait analysis. To reduce the disturbance caused by walking speed, the average preferred walking speed (PWS) [54] of the eight participants was selected for all subsequent test conditions. It was finally determined that the experiment would be carried out at a uniform velocity of 1.34m/s. In addition, in order to rule out the influence of some unexpected factors on the experimental results, before the start of the experiment, the participants were asked to adapt to walking with joint braces on the treadmill (the joint braces were limited to the main force leg and the main force legs of all participants was the right one), until they were familiar with the experimental specifications.

Before the start of the experiment, the equipment was checked and corrected. When the experiment started, the eight participants maintained a constant PWS of 1.34 m/s on the treadmill. Experiments were performed under the following conditions: Normal walking, walking with knee brace on unilateral side and walking with ankle brace on the unilateral side. Acceleration data on the left and right sides of the participants' back waist, hip joints and knee joints were collected, and data collection was carried out for each test condition. All experiments were repeated three times for each of the eight participants, and the completion of each group of experiments required a five-minute interval before the initiation of the next. The accelerometer transmitted data to the computer via Bluetooth for data processing.

3.2. Dataset

3.2.1. Dataset description

The work includes gait data of the same task in different states, which is used to verify the measurement method proposed in this paper. The data set contains gait signal data of eight different subjects in the laboratory. The acceleration sensors placed on the subjects' seven parts are used to record the acceleration data of three different walking states (normal, right knee joint brace, left knee joint brace).

3.2.2. Dataset validation

The benchmark datasets (MHEALTH, KFall) have been widely used in gait research with the standard time series dataset (UCR) [60–62]. The relevant comparison of datasets is listed in Table 1. These datasets have rich activity categories and data volumes, but they are usually used for the task classification. In the later research, we used our dataset in the research of DTW based evaluation method to realize the quantitative evaluation of abnormal state and normal state.

Table 1. Comparison of multiple gait related datasets.

Dataset	Number of tasks	Number of sensors	Type of data
Ours	3	7	Acceleration
MHEALTH	12	8	Acceleration, ECG, Gyroscope, Magnetic field
UCR-SGWZ	10	1	Acceleration
KFall	36	1	Acceleration, Gyroscope, Euler angle

3.3. Signal de-noising

In this study, acceleration sensors were used to collect the signals of the participants during walking, and then the DTW algorithm was used to process the signals. However, the DTW algorithm is sensitive to noise due to its operation characteristics and this noise would have a significant impact on the results without de-noising. Therefore, this study focuses on the DTW algorithm and introduces an improved smoothing function for de-noising optimization [55]. Figure 4 shows the acceleration signal before and after filtering at the knee joint. It is evident that the acceleration signal before filtering contains substantial noise but the de-noising effect of the improved wavelet threshold is ideal, and the acceleration curve after de-noising is smoother than that before.

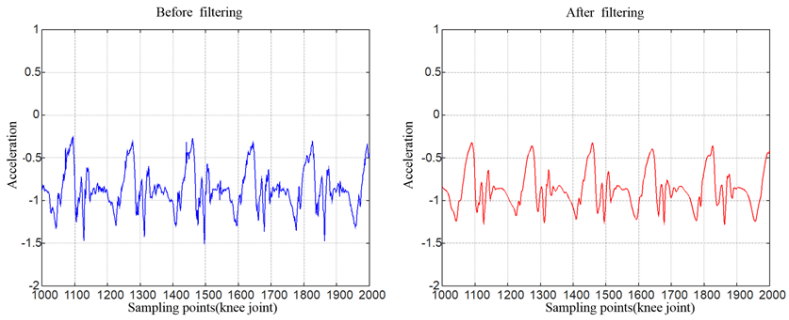

Figure 4. Original and filtered acceleration signal at the knee joint.

3.4. Stride division and acceleration trajectory

The gait has continuity and repetition, with a certain periodicity. The process cycle from a heel landing to the same heel landing again is called a complete gait cycle. In this paper, the piecewise linear function algorithm is used to average the acceleration trajectories of ten consecutive gait cycles at each joint of the participants. Figure 5 shows the Z-axis acceleration trajectories of different joints.

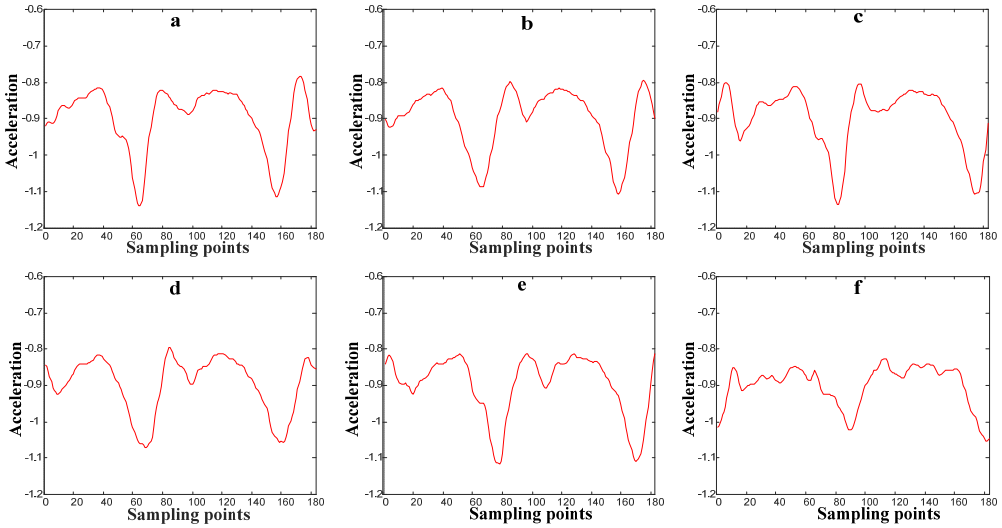

Figure 5. Acceleration trajectories at different joints (a): Left hip; (b): Left knee; (c): Left ankle; (d): Right hip joint; (e): Right knee; (f): Right ankle.

The gait has continuity and repetition, with a certain periodicity. The process cycle from a heel landing to the same heel landing again is called a complete gait cycle. In this paper, the piecewise linear function algorithm is used to average the acceleration trajectories of ten consecutive gait cycles at each joint of the participants. Figure 5 shows the Z-axis acceleration trajectories of different joints.

3.5. Dynamic time warping optimal path

When different joints are braced, the cumulative distance of the shortest path at each joint of the left and right legs is shown in Table 2.

Table 2. Cumulative distance of the shortest path at the left and right foot joints for different joint braces.

	Left and right hip joints	Left and right knee joints	Left and right ankle joints
Normal walk	4.0659	3.5835	4.7453
Knee brace	11.0882	17.9289	16.9012
Ankle brace	9.3747	5.8626	10.1942

Figure 6 shows the shortest path cumulative distance at the left and right foot joints braced by different joints. Table 2 and Figure 6 show that, in the case of normal walking, the $d_{Distance}$ at the hip, knee and ankle joints is smaller, while under the brace of the knee joint, compared to normal walking, the $d_{Distance}$ at the hip, knee and ankle joints is significantly higher.

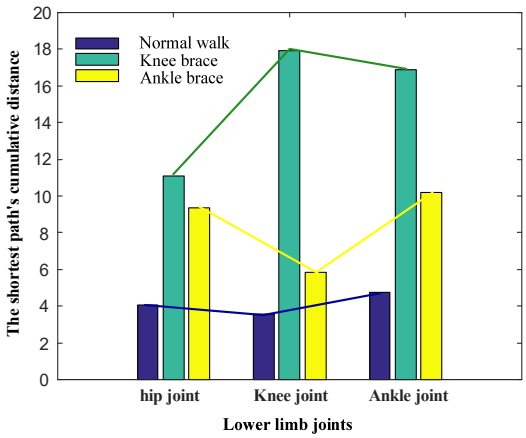

Figure 6. Shortest path's cumulative distance at the left and right foot joints.

The shortest path cumulative distance $d_{Distance}$ at each joint of the left and right feet for the different joint braces is shown in Table 3.

Figure 7 illustrates the shortest path cumulative distance $d_{Distance}$ at each joint of a unilateral leg, under the different joint braces. Figure 7 and Table 3 show that, with the ankle joint brace, the $d_{Distance}$ of the unbraced leg, which resembles normal walking process, is shorter than that of the braced leg, while it is the longest at the ankle joint of the braced leg. With the knee joint brace, the $d_{Distance}$ of the unbraced leg is shorter than that of the braced leg, while the $d_{Distance}$ at the knee joint of the braced leg appears to be the longest.

Table 3. Shortest path cumulative distance of left and right foot joints for different joint braces.

	Back waist	Left hip	Right hip	Left knee	Right knee	Left ankle	Right ankle
Knee brace	10.2009	6.4267	12.8661	6.5607	16.7190	6.2237	13.7090
Ankle brace	8.5659	6.6055	12.2558	5.1802	11.0747	6.8064	14.3978

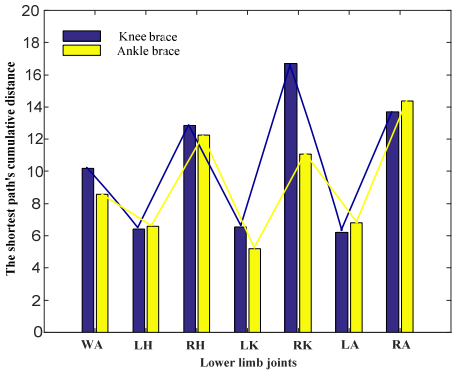

Figure 7. Cumulative shortest path distance at each joint of a single leg (WA: Waist; LH: Left hip; RH: Right hip; LK: Left knee; RK: Right knee; LA: Left ankle; RA: Right ankle)

3.6. Stability measurement results and analysis

The DTW algorithm allows us to assess quantitatively the size of each gait cycle and of different stages of the same gait cycle. In this study, it was used to evaluate the stability of bilateral lower limbs and the joints of the single leg under different joint braces (unbraced, ankle and knee brace), to study the influence of joint activities on lower limb gait stability. The three different bracing conditions (normal walking, ankle brace and knee brace) were compared. Based on the data distribution of the eight participants over ten consecutive gait cycles, the gait stability of the lower limbs on both sides and that between the lower limbs on unilateral side, as well as the average stride length were derived. The results after data normalization are shown in Tables 4 and 5, which list the mean and standard deviation of the bilateral stride stability metrics of the lower limbs braced by different joints.

3.6.1. Measurement of bilateral lower limb gait stability

The mean and standard deviation of the gait stability metrics during normal walking were 91.56 ± 1.08%, 92.13 ± 1.39 and 89.51 ± 2.13%. These figures indicate that gait stability during normal walking is good, and the disturbance of the joints to the gait movement is very small, so the stability index of normal gait is a high score.

When the ankle joint was braced, the gait stability index at the ankle joint decreased from 89.51% to 78.24% during normal walking, a decrease of 11.27 percentage points (pp). The stability index at the hip joint decreased from 91.26% to 81.28% during normal walking, which represents a decrease of 10.28 pp. The stability index at the knee joint decreased from 92.13% to 88.15% during normal walking, i.e., by 3.98 pp. This shows that the decrease of ankle joint mobility caused by the ankle joint brace caused a certain disturbance to normal walking, while the ankle joint mobility decreased and gait stability deteriorated. With the knee joint brace, the stability index at the knee joint decreased from 92.13% to 67.32% during normal walking, a decrease of 24.81 pp. At the hip joint, the stability index decreased from 91.26% to 76.58% during normal walking, a decrease of 14.98 pp, and from 89.51% to 69.15% at the ankle joint, namely 20.36 pp. These figures indicate that the decrease in the range of motion of the knee joint caused by the knee joint brace has a greater impact on gait stability, and in addition to the disturbance of the stability of the knee joint itself, the stability of the hip and ankle joints was also greatly affected.

Table 4. Mean and standard deviation of stability indexes of lower limb joints under different joint brace (%).

	Left and right hip joints	Left and right knee joints	Left and right ankle joints
Normal walk	91.56 ± 1.08	92.13 ± 1.39	89.51 ± 2.13
Knee brace	76.58 ± 3.66	67.32 ± 6.06	69.15 ± 5.28
Ankle brace	81.28 ± 1.71	88.15 ± 1.11	78.24 ± 2.64

The above data show that the decrease in joint range of motion caused by bracing the joints will inevitably lead to gait instability, which also results in a decrease in the corresponding stability index. These changes can be seen more clearly through the quantitative stability measure metrics (shown in

Figure 8). In a study of patients with knee arthritis by Sharon et al. [63], it was shown that patients with arthritis exhibited greater joint stiffness during walking than healthy individuals, and that increased joint stiffness may affect gait instability. Ro et al. [64] also pointed out in the quantitative assessment of gait after total knee arthroplasty that postoperative knee adduction moment and changes in knee flexion angle are the more obvious features. In each braced joint, the stability index decrease was the most pronounced, indicating that joint brace had a direct impact on the normal function of the joint and consequently affecting the stability of the entire lower limb. In addition, compared with normal walking, the knee joint brace caused greater disturbance to the gait stability, indicating that the knee joint has a stronger impact on the overall motion than the ankle joint.

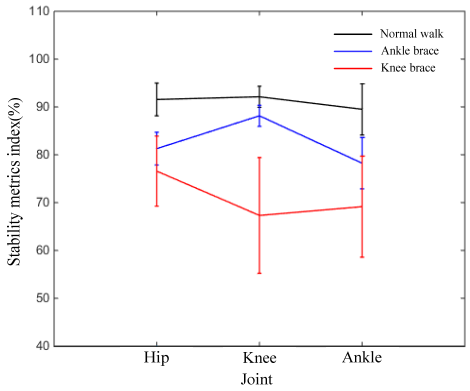

Figure 8. Numerical distribution of stability metrics under different joint braces.

3.6.2. Measurement of unilateral lower limb gait stability.

Table 5 lists the mean and variance of the unilateral stride stability metrics of lower limbs braced at different joints.

Under the ankle and knee joints were braced, the average value of the gait stability index, at the unbraced joint was more than 85%. Compared to the unbraced side, the standard deviation and average value of gait stability index of the right hip, knee and ankle on the knee-braced leg were 73.34 ± 4.41%, 66.71 ± 6.71% and 72.48 ± 4.62%, while the mean and standard deviation of the gait stability index of right hip, right knee and right ankle, on the ankle-braced leg were 76.53 ± 3.61%, 78.34 ± 2.81% and 72.43 ± 4.79%.

Under the ankle joint brace, the mean value of the gait stability index at the right ankle was the smallest, which was 72.43%, indicating that the ankle joint brace caused the greatest disturbance to the ankle joint. Under the knee joint brace, the mean value of the stability index of the right knee was the smallest at 66.71 ± 6.71%, indicating that the knee joint brace caused the greatest disturbance to the knee joint.

Table 5. Mean value and standard deviation of gait stability index at each joint of left and right feet under different joint brace (%).

	Back waist	Left hip	Right hip	Left knee	Right knee	Left ankle	Right ankle
Knee brace	78.62 ± 3.16	88.37 ± 1.39	73.34 ± 4.41	86.21 ± 1.71	66.71 ± 6.71	87.51 ± 1.26	72.48 ± 4.62
Ankle brace	83.31 ± 1.73	87.32 ± 1.39	76.53 ± 3.61	89.21 ± 0.85	78.34 ± 2.81	86.53 ± 1.96	72.43 ± 4.79

It can be seen from the above data combined with Figure 9 that the motion of the joints on the braced side is quite different to normal walking due to joints' limited range of motion, while the motion of the joints on the unbraced side is closer to that of normal walking. It can be seen that the joint brace leads to asymmetric movements on both sides during walking, resulting in a decrease in gait stability. This again confirms Ro et al.'s conclusion that the most significant difference in gait characteristics before and after surgery is bilateral symmetry [64]. In addition, the corresponding joints that were braced (for example, the braced right knee and the unbraced left knee) had the largest index difference, once again verifying the impact of decreased joint mobility on joint stability. Compared with the joint motion of the other bracing sides, the deviation of the joint motion at the knee joint was the largest.

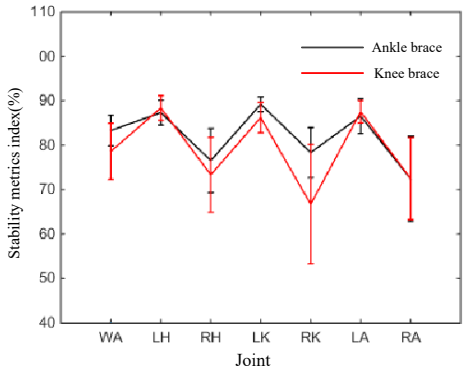

Figure 9. Numerical distribution of stability metrics under different joint braces.

In combination with the above experiments, the DTW algorithm is sensitive to small changes such as amplitude, which also enables even similar joint activities to obtain small difference measurements. Therefore, the quantitative gait evaluation method based on DTW cannot only distinguish the instability degree of different motion states, but also make the influence degree of each joint show obvious differences. For potential applications, it allows doctors to have accurate evaluation values in clinical diagnosis, which is of great significance for early clinical diagnosis of diseases with corresponding symptoms, as well as tracking and quantitative evaluation of the target site when recovering after surgery.

3.7. Limitations

In this study, normal individuals were selected as subjects to verify the feasibility of the DWT evaluation method. The limitation is the absence of data on patients with clinical or pathological cases, which may affect the diversity evaluation of subjects and the system's operational robustness. In addition, joint braces were conducted only on two major lower limb joints in the simulation of unstable gait, which may overlook other factors (including joints and muscle strength). These limitations curtail the broader impact and adoption of the proposed methodology for clinical settings, and require further research before the proposed evaluation methods can be used for disease diagnosis.

4. Conclusions

In order to accurately quantify the effect of joint motion on gait stability during walking, a DTW-based gait stability evaluation algorithm is proposed. Wearable sensors were used to collect acceleration signals at various joints, and an innovative calculation method of the stability metric index was used to quantify the data processed by DTW algorithm into an intuitive percentage score. In this paper, the improved DTW-based gait stability evaluation method provided effective information for the impact of joint motion on gait stability, and was validated experimentally through the comparison of participants under normal and braced-joint conditions. The proposed method does not rely on the subjective evaluation of experts and a large number of early trainings and can be applied to gait abnormality detection and limb rehabilitation monitoring. The limitations of this study, such as clinical trials on real pathological cases and other factors that affect gait parameters, need to be further studied. In future work, patients with lower limb pathological diseases or individuals with a history of lower limb diseases can be considered as subjects to determine differences in disease assessment and evaluate the impact of more factors, and to improve the effectiveness of the study and operational robustness with AI technology. In summary, our proposed gait evaluation method based on wearable acceleration sensor signals has potential importance for evaluating lower limb dysfunction, clinical training and rehabilitation.

Use of AI tools declaration

The authors declare they have not used Artificial Intelligence (AI) tools in the creation of this article.

Acknowledgments

This work was supported by the Zhejiang Provincial Natural Science Foundation of China (no. LY20E050011).

Conflict of interest

The authors declare no conflicts of interest.

References

1. G. M. Scalera, M. Ferrarin, M. Rabuffetti, Gait regularity assessed by wearable sensors: Comparison between accelerometer and gyroscope data for different sensor locations and walking speeds in healthy subjects, *J. Biomech.*, **113** (2020), 110115. https://doi.org/10.1016/j.jbiomech.2020.110115
2. Y. P. Demir, S. A. Yildirim, Different walk aids on gait parameters and kinematic analysis of the pelvis in patients with adult neuromuscular disease, *Neurosciences*, **24** (2019), 36–44. https://doi.org/10.17712/nsj.2019.1.20180316
3. Y. Wang, Z. Liu, J. Xu, W. Yan, Heterogeneous network representation learning approach for ethereum identity identification, *IEEE Trans. Comput. Soc. Syst.*, **10** (2023), 890–899. https://doi.org/10.1109/TCSS.2022.3164719
4. K. G. M. Quispe, W. S. Lima, D. M. Batista, E. Souto, MBOSS: A symbolic representation of human activity recognition using mobile sensors, *Sensors*, **18** (2018). https://doi.org/10.3390/s18124354
5. S. Bahadori, J. M. Williams, T. W. Wainwright, Lower limb kinematic, kinetic and spatial-temporal gait data for healthy adults using a self-paced treadmill, *Data Brief*, **34** (2021), 106613. https://doi.org/10.1016/j.dib.2020.106613
6. M. F. Antwi-Afari, H. Li, Fall risk assessment of construction workers based on biomechanical gait stability parameters using wearable insole pressure system, *Adv. Eng. Inf.*, **38** (2018), 683–694. https://doi.org/10.1016/j.aei.2018.10.002
7. H. Ohtsu, S. Yoshida, T. Minamisawa, N. Katagiri, T. Yamaguchi, T. Takahashi, et al., Does the balance strategy during walking in elderly persons show an association with fall risk assessment?, *J. Biomech.*, **103** (2020), 109657. https://doi.org/10.1016/j.jbiomech.2020.109657
8. J. R. Brickner, J. L. Garzon, K. A. Cimprich, Walking a tightrope: The complex balancing act of R-loops in genome stability, *Mol. Cell*, **82** (2022), 2267–2297. https://doi.org/10.1016/j.molcel.2022.04.014
9. J. C. Schrijvers, J. C. van den Noort, M. van der Esch, J. Dekker, J. Harlaar, Objective parameters to measure (in)stability of the knee joint during gait: A review of literature, *Gait Posture*, **70** (2019), 235–253. https://doi.org/10.1016/j.gaitpost.2019.03.016
10. J. N. Katz, K. R. Arant, R. F. Loeser, Diagnosis and treatment of hip and knee osteoarthritis: A Review, *J. Am. Med. Assoc.*, **325** (2021), 568–578. https://doi.org/10.1001/jama.2020.22171
11. M. Wang, X. Wang, C. Peng, S. Zhang, Z. Fan, Z. Liu, Research on EMG segmentation algorithm and walking analysis based on signal envelope and integral electrical signal, *Photonic Netwrk Commun.*, **37** (2019), 195–203. https://doi.org/10.1007/s11107-018-0809-1
12. S. Borel, P. Schneider, C. J. Newman, Video analysis software increases the interrater reliability of video gait assessments in children with cerebral palsy, *Gait Posture*, **33** (2011), 727–729. https://doi.org/10.1016/j.gaitpost.2011.02.012
13. S. Chakraborty, A. Nandy, T. Yamaguchi, V. Bonnet, G. Venture, Accuracy of image data stream of a markerless motion capture system in determining the local dynamic stability and joint kinematics of human gait, *J. Biomech.*, **104** (2020), 109718. https://doi.org/10.1016/j.gaitpost.2011.02.012

14. C. N. Armitano, H. J. Bennett, J. A. Haegele, S. Morrison, Assessment of the gait-related acceleration patterns in adults with autism spectrum disorder, *Gait Posture*, **75** (2020), 155–162. https://doi.org/10.1016/j.gaitpost.2019.09.002
15. Y. Shi, H. Li, X. Fu, R. Luan, Y. Wang, N. Wang, et al., Self-powered difunctional sensors based on sliding contact-electrification and tribovoltaic effects for pneumatic monitoring and controlling, *Nano Energy*, **110** (2023), 108339. https://doi.org/10.1016/j.nanoen.2023.108339
16. C. Mei, F. Gao, Y. Li, A determination method for gait event based on acceleration sensors, *Sensors*, **19** (2019), 5499. https://doi.org/10.3390/s19245499
17. J. Taborri, E. Palermo, S. Rossi, P. Cappa, Gait partitioning methods: A systematic review, *Sensors*, **16** (2016), 66. https://doi.org/10.3390/s16010066
18. H. Chen, F. Gao, C. Chen, T. Tian, Estimation of ankle angle based on multi-feature fusion with random forest, in *2018 37th Chinese Control Conference (CCC), IEEE*, (2018), 5549–5553.
19. M. D. Gor-García-Fogeda, R. Cano de la Cuerda, M. Carratalá Tejada, I. M. Alguacil-Diego, F. Molina-Rueda, Observational gait assessments in people with neurological disorders: A systematic review, *Arch. Phys. Med. Rehabil.*, **97** (2016), 131–140. https://doi.org/10.1016/j.apmr.2015.07.018
20. C. R. Brown, S. J. Hillman, A. M. Richardson, J. L. Herman, J. E. Robb, Reliability and validity of the visual gait assessment scale for children with hemiplegic cerebral palsy when used by experienced and inexperienced observers, *Gait Posture*, **27** (2008), 648–652. https://doi.org/10.1016/j.gaitpost.2007.08.008
21. C. H. Lee, S. H. Chen, B. C. Jiang, T. L. Sun, Estimating postural stability using improved permutation entropy via tug accelerometer data for community-dwelling elderly people, *Entropy*, **22** (2020), 354–365. https://doi.org/10.3390/e22101097
22. S. Majumder, M. J. Deen, Wearable IMU-based system for real-time monitoring of lower-limb joints, *IEEE Sensors J.*, **21** (2020), 8267–8275. https://doi.org/10.1109/JSEN.2020.3044800
23. J. Taborri, J. Keogh, A. Kos, A. Santuz, A. Umek, C. Urbanczyk, E. van der Kruk, S. Rossi, Sport biomechanics applications using inertial, force, and EMG sensors: A literature overview, *Appl. Bionic. Biomech.*, **27** (2020), 65–78. https://doi.org/10.1155/2020/2041549
24. A. Rajkumar, F. Vulpi, S. R. Bethi, H. K. Wazir, P. Raghavan, V. Kapila, Wearable Inertial Sensors for Range of Motion Assessment, *IEEE Sensors J.*, **20** (2020), 3777–3787. https://doi.org/10.1109/JSEN.2019.2960320
25. J. Liu, T. Lockhart, S. Kim, Prediction of the spatio-temporal gait parameters using inertial sensor, *J. Mech. Med. Biol.*, **18** (2018), 121–135. https://doi.org/10.1142/S021951941840002X
26. S. Bahadori, J. M. Williams, T. W. Wainwright, Lower limb kinematic, kinetic and spatial-temporal gait data for healthy adults using a self-paced treadmill, *Data Brief*, **34** (2021), 106613. https://doi.org/10.1016/j.dib.2020.106613
27. J. Soulard, J. Vaillant, R. Balaguier, N. Vuillerme, Spatio-temporal gait parameters obtained from foot-worn inertial sensors are reliable in healthy adults in single- and dual-task conditions, *Sci. Rep.*, **11** (2021), 10229. https://doi.org/10.1038/s41598-021-88794-4
28. S. M. Moghadam, T. Yeung, J. Choisne, A comparison of machine learning models' accuracy in predicting lower-limb joints' kinematics, kinetics, and muscle forces from wearable sensors, *Sci. Rep.*, **13** (2023), 5046. https://doi.org/10.1038/s41598-023-31906-z

29. G. Salatino, E. Bergamini, T. Marro, P. Gentili, M. Iosa, D. Morelli, et al., Gait stability assessment in Down and Prader-Willi syndrome children using inertial sensors, *Gait Posture*, **49** (2016), S16. https://doi.org/10.1016/j.gaitpost.2016.07.046
30. J. Johansson, A. Nordström, P. Nordström, Greater fall risk in elderly women than in men is associated with increased gait variability during multitasking, *J. Am. Med.*, **17** (2016), 535–540. https://doi.org/10.1016/j.jamda.2016.02.009
31. N. J. Nelms, C. E. Birch, D. H. Halsey, M. Blankstein, B. D. Beynnon, Assessment of early gait recovery after anterior approach compared to posterior approach total hip arthroplasty: A smartphone accelerometer-based study, *J. Arthroplasty*, **35** (2019), 125–138. https://doi.org/10.1016/j.arth.2019.09.030
32. P. Tamburini, F. Storm, C. Buckley, M. C. Bisi, R. Stagni, C. Mazzà, Moving from laboratory to real life conditions: Influence on the assessment of variability and stability of gait, *Gait Posture*, **59** (2018), 248–252. https://doi.org/10.1016/j.gaitpost.2017.10.024
33. N. Muthukrishnan, J. J. Abbas, N. Krishnamurthi, A wearable sensor system to measure step-based gait parameters for parkinson's disease rehabilitation, *Sensors*, **20** (2020), 6417. https://doi.org/10.3390/s20226417
34. J. Y. Wang, D. W. Gong, H. C. Luo, W. B. Zhang, L. Zhang, H. Zhang, et al., Measurement of step angle for quantifying the gait impairment of parkinson's disease by wearable sensors: Controlled study, *JMIR mHealth uHealth*, **8** (2020), 10–25. https://doi.org/10.2196/16650
35. A. Nguyen, N. Roth, N. H. Ghassemi, J. Hannink, T. Seel, J. Klucken, et al., Development and clinical validation of inertial sensor-based gait-clustering methods in Parkinson's disease, *J. Neuroeng. Rehabil.*, **16** (2019), 147–159. https://doi.org/10.1186/s12984-019-0548-2
36. P. Caliandro, C. Conte, C. Iacovelli, A. Tatarelli, S. F. Castiglia, G. Reale, et al., Exploring risk of falls and dynamic unbalance in cerebellar ataxia by inertial sensor assessment, *Sensors*, **19** (2019), 5571. https://doi.org/10.3390/s19245571
37. P. Tamburini, F. Storm, C. Buckley, M. C. Bisi, R. Stagni, C. Mazza, Moving from laboratory to real life conditions: Influence on the assessment of variability and stability of gait, *Gait Posture*, **59** (2018), 248–252. https://doi.org/10.1016/j.gaitpost.2017.10.024
38. M. Diopa, A. Rahmani, A. Belli, V. Gautheron, A. Geyssant, J. Cottalorda, Influence of speed variation and age on the asymmetry of ground reaction forces and stride parameters of normal gait in children, *J. Pediatric Orthopaedics-Part B*, **13** (2004), https://doi.org/10.1097/01202412-200409000-00005
39. J. Zhao, Y. Lv, Output-feedback robust tracking control of uncertain systems via adaptive learning, *Int. J. Control Autom. Syst.*, **21** (2023), 1108–1118. https://doi.org/10.1007/s12555-021-0882-6
40. Y. Shi, L. Li, J. Yang, Y. Wang, S. Hao, Center-based transfer feature learning with classifier adaptation for surface defect recognition, *Mech. Syst. Signal Process.*, **188** (2023), 110001. https://doi.org/10.1016/j.ymssp.2022.110001
41. Z. Liu, D. Yang, Y. Wang, M. Lu, R. Li, EGNN: Graph structure learning based on evolutionary computation helps more in graph neural networks, *Appl. Soft Comput.*, **135** (2023), 110040. https://doi.org/10.1016/j.asoc.2023.110040
42. C. Tian, Z. Xu, L. Wang, Y. Liu, Arc fault detection using artificial intelligence: Challenges and benefits, *Math. Biosci. Eng.*, **20** (2023), 12404–12432. https://doi.org/10.3934/mbe.2023552

43. A. S. Alharthi, S. U. Yunas, K. B. Ozanyan, Deep learning for monitoring of human gait: A review, *IEEE Sensors J.*, **19** (2019), 9575–9591. https://doi.org/10.1109/JSEN.2019.2928777
44. T. Yao, F. Gao, Q. Zhang, Y. Ma, Multi-feature gait recognition with DNN based on sEMG signals, *Math. Biosci. Eng.*, **18** (2021), 3521–3542. 18(4). https://doi.org/10.3934/mbe.2021177
45. E. Sansano, R. Montoliu, Ó. B. Fernández, A study of deep neural networks for human activity recognition, *Comput. Intell.*, **36** (2020), 1113–1139. https://doi.org/10.1111/coin.12318
46. J. N. Mogan, C. P. Lee, K. M. Lim, K. S. Muthu, Gait-ViT: Gait recognition with vision transformer, *Sensors*, **22** (2022), 362. https://doi.org/10.3390/s22197362
47. R. Moe-Nilssen, A new method for evaluating motor control in gait under real-life environmental conditions. Part 1: The instrument, *Clin. Biomech.*, **13** (1998), 320–327. https://doi.org/10.1016/S0268-0033(98)00089-8
48. M. I. Esfahani, M. A. Nussbaum, Using smart garments to differentiate among normal and simulated abnormal gaits, *J. Biomech.*, **93** (2019), 70–76. https://doi.org/10.1016/j.jbiomech.2019.06.009
49. M. S. Jia, T. H. Li, J. Wang, Audio fingerprint extraction based on locally linear embedding for audio retrieval system, *Electronics*, **9** (2020), 238–253. https://doi.org/10.1016/j.imu.2018.10.002
50. P. A. Semblantes, V. H. Andaluz, J. Lagla, F. A. Chicaiza, A. Acurio, Visual feedback framework for rehabilitation of stroke patients, *Inf. Med. Unlocked*, **13** (2018), 41–50. https://doi.org/10.1016/j.imu.2018.10.002
51. C. J. Su, C. Y. Chiang, J. Y. Huang, Kinect-enabled home-based rehabilitation system using dynamic time warping and fuzzy logic, *Appl. Soft Comput.*, **22** (2014), 652–666. https://doi.org/10.1016/j.asoc.2014.04.020
52. J. Minsu, D. Kim, Y. Kim, K. Jaehong, Automated dance motion evaluation using dynamic time warping and Laban movement analysis, in *IEEE International Conference on Consumer Electronics*, (2017), 141–142.
53. R. Haghighi Osgouei, D. Soulsby, F. Bello, Rehabilitation exergames: Use of motion sensing and machine learning to quantify exercise performance in healthy volunteers, *JMIR Rehabil. Assistive Technol.*, **7** (2020), e17289. https://doi.org/10.2196/17289
54. I. Hagoort, N. Vuillerme, T. Hortobágyi, C. J. Lamoth, Outcome-dependent effects of walking speed and age on quantitative and qualitative gait measures, *Gait Posture*, **93** (2022), 39–46. https://doi.org/10.1016/j.gaitpost.2022.01.001
55. Z. Yan, X. Xu, Y. Wang, T. Li, B. Ma, L. Yang, et al., Application of ultrasonic doppler technology based on wavelet threshold denoising algorithm in fetal heart rate and central nervous system malformation detection, *World Neurosurg.*, **30** (2020), 168–179. https://doi.org/10.1016/j.wneu.2020.10.030
56. R. Takeda, S. Tadano, M. Todoh, M. Morikawa, M. Nakayasu, S. Yoshinari, Gait analysis using gravitational acceleration measured by wearable sensors, *J. Biomech.*, **42** (2009), 223–233. https://doi.org/10.1016/j.jbiomech.2008.10.027
57. Y. Liu, G. Yin, The Delaunay triangulation learner and its ensembles, *Comput. Stat. Data Anal.*, **152** (2020), 1121–1135. https://doi.org/10.1016/j.csda.2020.107030
58. X. Yu, S. Xiong, A dynamic time warping based algorithm to evaluate kinect-enabled home-based physical rehabilitation exercises for older people, *Sensors*, **19** (2019), 2882. https://doi.org/10.3390/s19132882

59. T. Seel, J. Raisch, T. Schauer, IMU-based joint angle measurement for gait analysis, *Sensors*, **14** (2014), 6891–6909. https://doi.org/10.3390/s140406891
60. V. B. Semwal, A. Gupta, P. Lalwani, An optimized hybrid deep learning model using ensemble learning approach for human walking activities recognition, *J. Supercomput.*, **77** (2021), 12256–12279. https://doi.org/10.1007/s11227-021-03768-7
61. X. Yu, J. Jang, S. Xiong, A large-scale open motion dataset (KFall) and Benchmark algorithms for detecting pre-impact fall of the elderly using wearable inertial sensors, *Front. Aging Neurosci.*, **13** (2021), 692865. https://doi.org/10.3389/fnagi.2021.692865
62. R. J. Kate, Using dynamic time warping distances as features for improved time series classification, *Data Mining Knowl. Discovery*, **30** (2015), 283–312. https://doi.org/10.1007/s10618-015-0418-x
63. S. J. Dixon, R. S. Hinman, M. W. Creaby, G. Kemp, K. M. Crossley, Knee joint stiffness during walking in knee osteoarthritis, *Arth. Care Res.*, **62** (2010), 38–44. https://doi.org/10.1002/acr.20012
64. D. H. Ro, T. Kang, D. Han, D. Y. Lee, H. S. Han, M. C. Lee, Quantitative evaluation of gait features after total knee arthroplasty: Comparison with age and sex-matched controls, *Gait Posture*, **75** (2020), 78–84. https://doi.org/10.1016/j.gaitpost.2019.09.026

AIMS Press